Sequential installation of Fe(ii) complexes in MOFs: towards the design of solvatochromic porous solids

Florian Moreau, Jérôme Marrot, Frédéric Banse, Christian Serre, Antoine Tissot

Sequential installation of Fe(II) complexes in MOFs: towards the design of solvatochromic porous solids

Florian Moreau,[a] Jérôme Marrot,[b] Frédéric Banse,[c] Christian Serre,[a*] Antoine Tissot[a*]

a. Institut des matériaux poreux de Paris, École normale supérieure, ESPCI Paris, CNRS, PSL University, 75005 Paris, France.

b. Institut Lavoisier de Versailles, UVSQ, Paris Saclay University, Versailles, France.

c. Université Paris-Saclay, CNRS, Institut de Chimie Moléculaire et des Matériaux d'Orsay, 91405 Orsay, France.

Abstract: Fe(II) coordination complexes have been anchored on robust Metal-Organic Frameworks secondary building units using a sequential installation strategy. The coordination sphere around Fe(II) has been modulated upon sorption of alcohols in the pores of the MOF, leading to a reversible colour change from orange to red. In the case of MFU-4l, a preferential adsorption of MeOH has been observed, evidencing the fact that the host matrix can be used for pre-concentrating a targeted analyte, which may be beneficial for the design of sensing devices.

Introduction

The design of volatile organic compounds (VOCs) chemosensors, i.e. solids which undergo a measurable change of their physical properties upon interaction with a targeted molecule is of great interest for environmental applications.[1,2] Porous switchable compounds are promising candidates for sensing, as their physical properties -for example their color- can be tuned upon guest sorption. Metal-Organic Frameworks (MOFs) are highly tunable porous solids, which can present outstanding sorption properties, combining high uptakes with important selectivities towards specific VOCs.[3–6] In some cases, their physical properties, such as their color, emissive or magnetic properties can evolve upon guest sorption.[7–13] However, switchable MOFs often lack of an adequate chemical stability for being used in real chemosensing applications.[14] In order to overcome this issue, an alternative strategy consists of loading molecular species, such as isomerizable or redox/pH responsive organic molecules or switchable coordination complexes, inside the pores of chemically stable MOFs.[15] To this end, spin crossover (SCO) complexes are promising candidates of switchable objects that can undergo a low-spin (LS) $\leftrightarrow$ high-spin (HS) conversion upon external stimuli such as temperature, pressure, light or chemisorption, accompanied by a change of magnetic, structural and optical properties.[16] The loading of SCO complexes in porous architectures has been first studied using oxalate-based networks, in which the complexes act as templates for the framework synthesis, resulting in non-porous hybrid structures.[17–19] Few examples of SCO complexes loaded in pre-synthesized MOFs have also been described.[20–22] In these cases, the limited MOF stability in presence of water and/or solvents may however prevent studying the effect of solvent or vapor loading on the spin state of the guest complexes. Recently, some of us have reported the loading of $Fe^{III}(sal_2trien)^+$ complexes into the water stable mesoporous aluminum trimesate MIL-100(Al) (MIL stands for Matériaux de l'Institut Lavoisier) using a bottle-in-a-ship strategy.[23] A reversible switching between HS and LS states at room temperature has been evidenced upon several water sorption-desorption cycles, evidencing the potential of such hybrid solids for sensing. However, this strategy does not allow controlling the location of the guest molecules in the pores, particularly when the pore size

largely exceeds the dimensions of the complex, making the switching properties of the compound barely predictable. This issue might be circumvented by anchoring, covalently or through coordination bonds, the guest complexes on the host matrix.

The post-synthetic modification of MOFs, either using organic linkers possessing free coordination sites or by anchoring coordinating moieties on secondary building units (SBUs), has been widely explored.[24,25] In addition, some spin crossover complexes can be functionalized with coordinating groups such as amines or carboxylic acids. For example, $Fe^{II}(HBPI)_2(ClO4)_2$ (HBPI = 2,6-bis(1H-pyrazol-1-yl)isonicotinic acid) is a molecular complex presenting both a spin transition close to room temperature and two free pending carboxylic acids on the linker.[26,27] This complex is a variation of $Fe(BPP)_2X_2$ complexes (BPP=bispyrazolpyridine derivatives) that often present a spin crossover in solution, which can depend on the nature of the solvent, making them appealing for solvent sensing.[28–31] Therefore, taking into account the ability of Zn(II), Al(III) or Zr(IV)-based MOFs to coordinate carboxylate groups on SBUs possessing labile positions, we have anchored $[Fe^{II}(BPI)(HBPI)(ClO_4)_2]^-$, name thereafter **1**, in water-stable MOFs presenting large enough pores to accommodate the complex, namely MFU-4l and MIL-100(Al) using a sequential installation strategy (Scheme 1). MFU-4l is a Zn^{II} triazolate microporous framework with two types of cubic cages with similar dimensions (15.5 Å sides), their vertices being occupied by Kuratowsky type secondary building units (SBUs) $Zn_5(BTDD)_6X_4$ (X= Cl-, BTDD=bis(1H-1,2,3-triazolo[4,5-b],-[4',5'-i])dibenzo[1,4]dioxin) while half of the cages exhibit 8 labile Cl ligands from the SBUs pointing towards their centers (see Figure S1).[32] The framework of MIL-100(Al) is constituted of 2 types of large cages (24 and 27 Å) with microporous windows (5.5 and 8.5 Å), the SBUs being oxocentered trimers of Al octahedra $Al_3O(H_2O)_2(OH)$ with a central μ3-oxo, 6 bridging carboxylates, and terminal labile H_2O or OH^- ligands pointing towards the center of windows (see Figure S2).[33,34] The color change of the functionalized **1**⊂MOF compounds dispersed in different solvents at room temperature has then been investigated, which is a preliminary step toward the sensing of VOCs in gas phase.

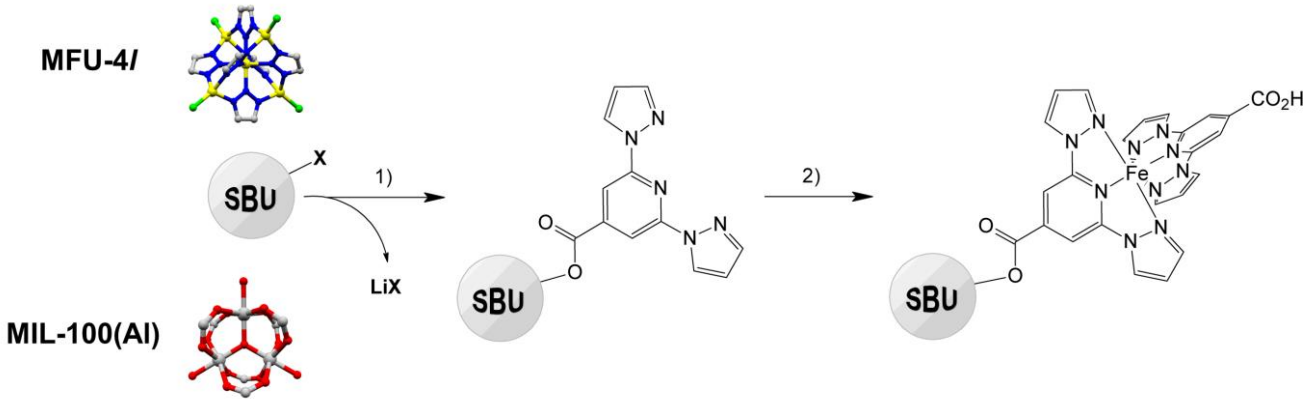

Scheme 1. Sequential installation strategy for pore functionalisation with anchored **1** complexes. 1) BPI.Li, MeOH, RT, 16-36h, 2) $Fe(ClO_4)_2.xH_2O$, HBPI, EtOH, RT, 16h.

Results and discussion

- Synthesis and characterization of spin crossover functionalized MOFs

The two MOFs selected in this study present large pores (>15 Å) that allow the sequential installation of coordination complexes **1** within their frameworks while retaining porosity. They also possess labile positions on their SBUs and in both cases, the SBU-terminal -X groups can be substituted by anionic species such as carboxylates. For the synthesis of **1**⊂MOF hybrid solids, MOFs were first soaked in a methanolic solution containing BPI.Li. After subsequent washing with MeOH, the amount of anchored BPI- was evaluated using ^{1}H NMR of the digested solid, indicating an average loading of 0.6 BPI^- linkers per SBU for MIL-100(Al) ($Al_3O(OH)_{0.4}(H_2O)_2(BTC)_2(BPI)_{0.6}$) and 2 BPI^- linkers for MFU-4l ($Zn_5(BTDD)_3Cl_2(BPI)_2$) (See ESI). Concomitantly, the amount of chlorine in MFU-4l decreases according to EDS, which indicates that the Cl^- anions coordinated to the SBU are replaced by BPI^-. In a second step, the solids were redispersed in EtOH in which $Fe^{II}(ClO_4)_2$ and HBPI were sequentially added. The addition of Fe^{II} and HBPI in the dispersion was accompanied with a gradual color change of the solid from white/clear brown to deep red, indicating the formation of $[(BPI)Fe(HBPI)]^+$-type complexes. Finally, the red solids were washed with EtOH and acetone and dried under vacuum at room temperature. The formula of the loaded solids is $[Al_{2.7}Fe_{0.3}O(OH)_{0.4}(H_2O)_2(BTC)_2][(BPI)_{0.6}Fe_{0.6}(BPI)_{0.5}(ClO_4)_{1.2}]$ for **1**⊂MIL-100(Al) and $Zn_5(BTDD)_3Cl_2[(BPI)_2Fe_2(HBPI)_{1.5}(ClO_4)_4]$ for **1**⊂MFU-4l according to ^{1}H NMR, EDS and TGA analysis (See ESI), which is in good agreement with the amount of linker anchored on the first step. The electroneutrality of the compounds is ensured by the loading of perchlorate anions in the solids. In the case of **1**⊂MIL-100(Al), the Fe/Al ratio measured by EDS exceeds the one expected from the loading of the SCO complex into the pores and results probably from a partial substitution of Al^{III} by Fe^{III} in the framework during the formation of the complex (See ESI).

The host MOFs exhibited PXRD patterns and N_2 sorption isotherms in agreement with the reported ones.[32,34] PXRD measurements on the loaded solids indicated that their crystallinity was not affected by the loading process (See Figure 1). Moreover, N_2 sorption isotherms at 77 K evidenced that a partial porosity was retained on the loaded MOFs, with BET surface areas decreasing from 1670 to 1050 m^2g^{-1} for MIL-100(Al) and 2730 to 650 m^2g^{-1} for MFU-4l (See Figure 2). The much larger drop in porosity for MFU-4l compared to MIL-100(Al), despite similar densities of complex **1** loaded in their pores (0.65 and 0.68 complexes/nm^3 for **1**⊂MIL-100(Al) and **1**⊂MFU-4l, respectively) can be attributed to differences in cages systems. Indeed in **1**⊂MFU-4l half of the -Cl groups from the SBUs have been replaced by anchored **1** complexes thus filling half of the pores of the framework and blocking the communication between the empty pores, whereas in MIL-100(Al), such pore blocking shall occur to a much lesser extent due to the framework topology. In addition to the decrease of sorption capacity, pore size distributions calculated by DFT evidenced in both cases a decrease of the average pore size during the loading process, which is consistent with a partial pore filling by coordination complexes (See Figures S5-6). The sequential installation of the complex **1** in the pores of the MOFs has further been evidenced by vibrational spectroscopy. Infrared spectra of the loaded MOFs unambiguously presented typical vibrations of the molecular complex **1** at 1705, 1625, 1573, 1526, 1404 cm^{-1} and of ClO_4^- anions at 1080 cm^{-1} (see Figure 3 and ESI). In particular, the vibration at 1625 cm^{-1} corresponds to the ν(C=N) vibration band of the HBPI linker coordinated to Fe(II) (ν(C=N)~1610 cm^{-1} for free HBPI/BPI-). The relative intensity of the vibration band at 1705 cm^{-1}, which corresponds to the vibration of the ν(COOH) group in **1**, was less intense in **1**⊂MIL-100(Al) and **1**⊂MFU-4l than in $Fe(HBPI)_2(ClO_4)_2$. It confirms the partial deprotonation of the HBPI linker in

1⊂MOF, in line with the first step of the installation strategy where BPI- is anchored to the MOFs inorganic building unit.

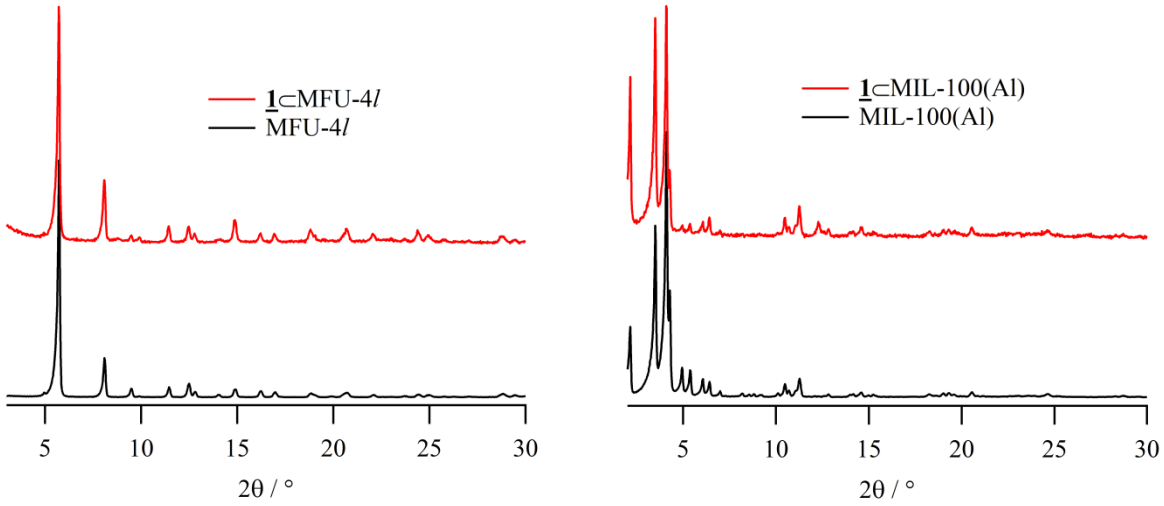

Figure 1: X-ray powder diffraction patterns (Cu Kα radiation) of MFU-4l and **1**⊂MFU-4l (left) and of MIL-100(Al) and **1**⊂MIL-100(Al) (right)

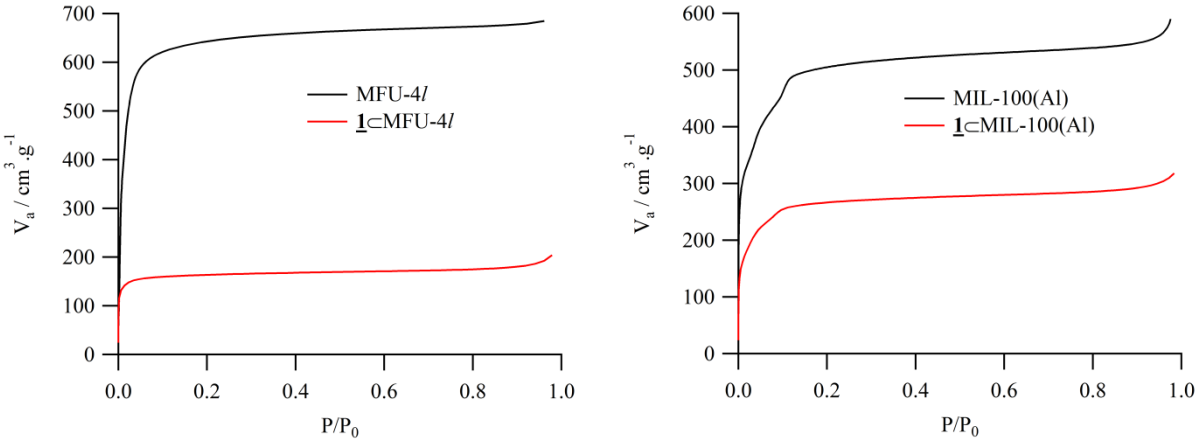

Figure 2: Comparison of 77 K N_2 sorption isotherms of MFU-4l and **1**⊂MFU-4l (left) and of MIL-100(Al) and **1**⊂MIL-100(Al) (right)(P_0=1 atm)

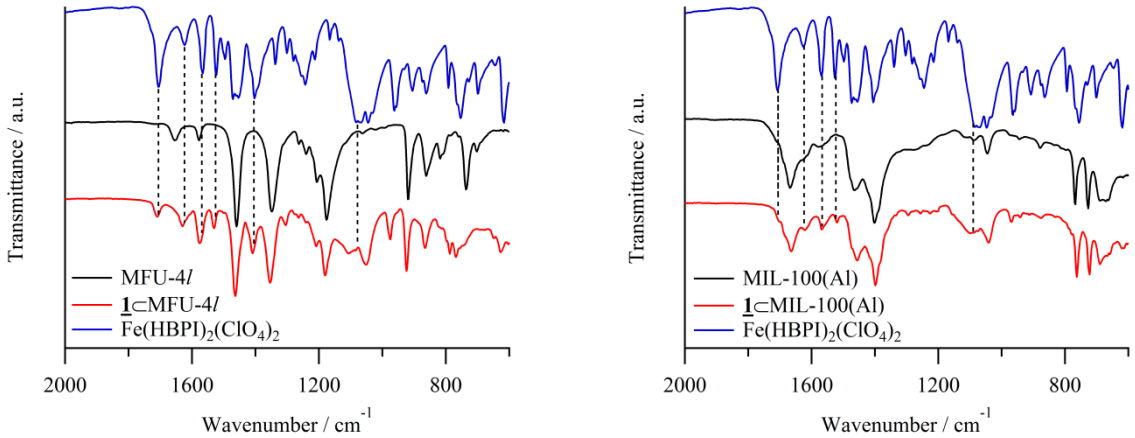

Figure 3: Infrared spectra of $Fe(HPI)_2(ClO_4)_2$, MFU-4l and **1**⊂MFU-4l (left) and of $Fe(HPI)_2(ClO_4)_2$, MIL-100(Al) and **1**⊂MIL-100(Al) (right)

- Solvatochromic behaviour of **1**⊂MOFs

During the washing/drying steps, the color of the samples changed from red to orange depending on the solvation state of the compound (acetone or EtOH), which is a first indication that the spin state and/or the coordination sphere of the loaded complexes can be modulated by solvent sorption. Therefore, UV-Visible spectra of the solids dispersed in several solvents have been measured. **1**⊂MOFs compounds exhibited an absorption band located at 450 nm in most solvents, except in MeOH or EtOH where the transition is located at 500-520 nm (see Figure 4). This difference may be explained by either (1) a spin change, as the MLCT transitions of Fe(II) complexes are often shifted towards lower energy upon HS-LS transition or (2) a solvation effect or (3) a change of the coordination environment around Fe(II).

In order to discriminate between these hypotheses, temperature dependent UV-Vis spectra of $Fe^{II}(HBPI)_2(ClO_4)_2$ in acetone have been measured (see Figure S10). A gradual thermal spin crossover centered around 285 K was observed, which is in line with previous results from the literature.[35] Upon the HS-LS conversion, the Fe(II) MLCT absorption band gained in intensity but its position remained almost unchanged (459 nm at 320 K vs. 464 nm at 210 K).[29] Therefore, the spin crossover phenomenon cannot explain the red shift of the absorption observed in alcohols. This is further supported by magnetization measurements performed on **1**⊂MIL-100(Al) and **1**⊂MFU-4l dispersed in EtOH that confirms that Fe(II) is HS in both compounds (see Figure S22). In order to check the effect of solvation on the color of $[Fe(HBPI)_2]^{2+}$, we prepared these complexes in several solvents by mixing $Fe(ClO_4)_2$ with a large excess of HBPI. In all cases, orange solutions were obtained with a maximum of the MLCT absorption peak located around 460 nm. Large differences in intensities were observed, indicating that the spin state of the complexes might depend on the solvent at RT (see Figure S11). However, this experiment evidenced that the red species observed in the MOF are not likely to correspond to $[Fe(HBPI)_2]^{2+}$ complexes where Fe^{II} is surrounded by 6 N atoms from the linker in a pseudo-octahedral geometry. Then, we have performed titration experiments by adding progressive amount of 1-BPP or HBPI in a solution of Fe^{II} in acetone or EtOH. With 1-BPP, a progressive increase in the MLCT absorption band intensity is noticed upon addition of the linker, without any shift of the band position. In acetone, a plateau is obtained after the addition of 2 equivalents of 1-BPP, suggesting a quantitative formation of $Fe(1\text{-}BPP)_2^{2+}$ species (see Figure S12). On the opposite, in EtOH the intensity increases progressively and no saturation is reached after the addition of 4 equivalents of 1-BPP, indicating that the coordination of 1-BPP to Fe^{II} is less favored, probably due to the higher complexing ability of EtOH compared to acetone (see Figure S13). Using HBPI and acetone as solvent, a similar trend is observed, corresponding to quantitative formation of $[Fe(HBPI)_2]^{2+}$ complexes without any detectable intermediate species (see Figure S14). On the opposite, when using HBPI and EtOH as solvent, a red compound quickly precipitated for molar ratios $HBPI/Fe^{II}$ close to one, as evidenced by the baseline jump in the UV-Visible spectra (see Figure S15). With more diluted solution, no precipitation occurred but a mixture between two species with maximum absorption at 460 nm and 500 nm respectively was observed, depending on the concentration and the molar ratio $HBPI/Fe^{II}$ (see Figure S16). At high dilution and with a large excess of HBPI, a red complex absorbing at 500 nm was quantitatively obtained (see Figure S17). As its absorption spectrum well corresponds to the one of **1**⊂MOFs compounds dispersed in alcohols, we can hypothesize that the same species were obtained in both experiments. In order to identify it, the solid was crystallized by slow evaporation of a methanolic solution containing Fe^{II} and HBPI. Dark red crystals were obtained and their structure was determined by single crystal XRD. In this compound, Fe(II) presents a

coordination sphere that is different from $[Fe^{II}(HBPI)_2](ClO_4)_2$: each Fe center is coordinated by 3 N atoms from one BPI^- linker, one COO^- group from a second BPI^- linker and 2 MeOH molecules, giving rise to a 1D coordination polymer (**2**, see ESI). Solid state UV-Vis spectra collected with an integration sphere for $[Fe^{II}(1\text{-}BPP)_2](ClO_4)_2$ and **2** evidenced that the FeN_6 coordination sphere of HS $[Fe^{II}(1\text{-}BPP)_2](ClO_4)_2$ corresponds to a transition centered at 430 nm, while the FeN_3O_4 coordination sphere of **2** corresponds to a transition centered at 510 nm (see Figure S18). In addition, Nikovskiy et al. recently reported a molecular structure presenting a similar coordination sphere, which is also associated to a red color while Fe(II) is in the HS state.[36]

In summary, the color change observed upon sorption of alcohols in the MOFs is probably not related to a spin state change or an effect of solvation without modification of the Fe^{II} coordination sphere but is likely to be associated to a coordination switch of one BPI ligand, giving rise to a red HS Fe(II) complex where one BPI linker is coordinated to the Fe^{II} through its 3 N atoms and the other one through the carboxylic acid group, while alcohol molecules can complete the coordination sphere.

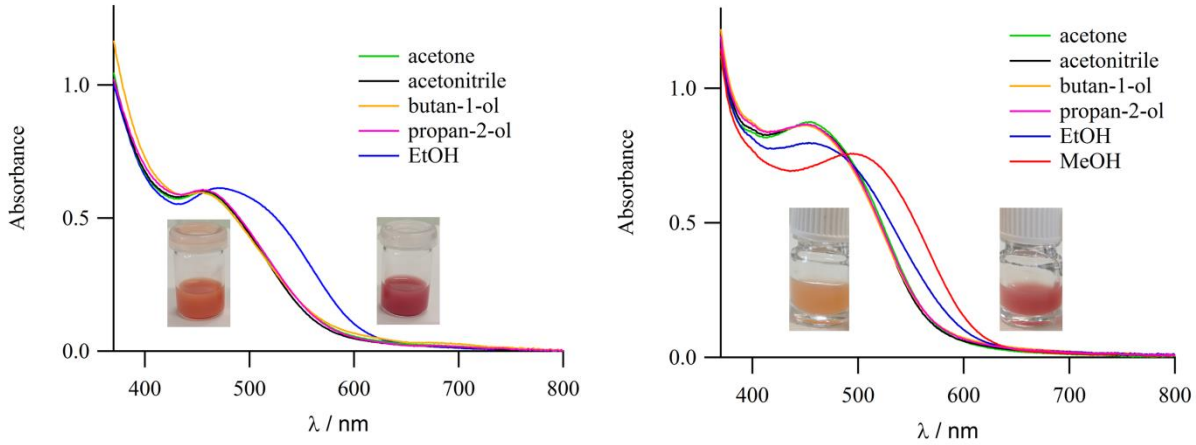

Figure 4: UV-Vis spectra at room temperature of **1**⊂MIL-100(Al); inset: pictures of **1**⊂MIL-100(Al) dispersed in acetone (orange) and EtOH (red) (left) and **1**⊂MFU-4l (right) dispersed in different solvents; inset: pictures of **1**⊂MFU-4l dispersed in acetone (orange) and MeOH (red)

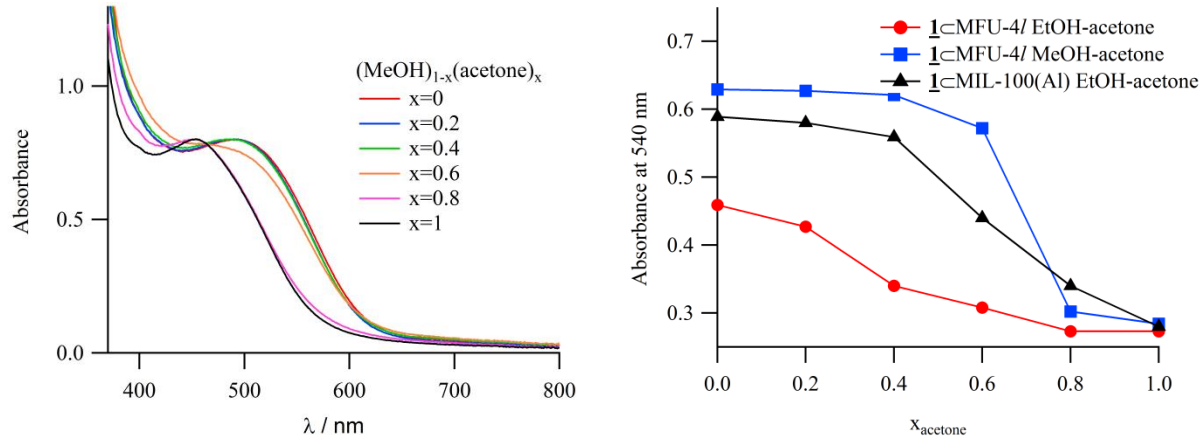

Figure 5: UV-Vis spectra at room temperature of **1**⊂MFU-4l in methanol-acetone solvent mixtures (left) and absorbance at 540 nm in different solvent mixtures for **1**⊂MIL-100(Al) and **1**⊂MFU-4l (right)

For all the solvents tested, the solutions remained perfectly clear after centrifugation, evidencing that no leaching of the metal complex occurred during the dispersion process. Moreover, the MOF

crystallinity was not affected by the dispersion in solvents. The samples that were first dispersed in alcohols did recover the orange color after drying and redispersing in acetone, indicating that the switching process is overall reversible (see Figure S19). However, a decrease of the MLCT band intensity is observed after several dispersion/drying cycles (ca. 10% per cycle), probably due to the partial leaching of HBPI when the solids are dispersed in alcohols.

UV-Vis spectra have then been recorded using acetone-alcohol mixtures. For these experiments, the sample was stirred for few minutes before the measurements to allow the diffusion of the solvent molecules in the pores up to a stationary state (see Figure S20). Different behaviors could be observed depending on the MOF-alcohol combination. In **1**⊂MIL-100(Al), a gradual evolution between the states corresponding to the solid dispersed in pure alcohol and pure acetone was observed (see Figure S21). In contrast, in the case of **1**⊂MFU-4l dispersed in MeOH/acetone mixtures, the transition was abrupt and occurred at a composition corresponding to 20% of MeOH in acetone (see Figure 5). This observation suggests that MFU-4l is likely to adsorb preferentially MeOH compared to acetone while in the other cases, the composition of the adsorbed solvent is close to the one of the dispersant.

When considering the water vapor sorption properties of MFU-4l and MIL-100(Al), it is clear from previous studies that MFU-4l is a more hydrophobic material at low humidity level.[37,38] However, the steepness of the water sorption isotherm observed for MFU-4l indicates that the appearance of an H-bond network in the pores is favored once guest molecules reach binding sites as partial pressure increases, possibly thanks to the oxygen atoms on the dioxin core of the linker that can act as H-Bond acceptors. In such a case, methanol, due to its small size and its H-bond donor nature, might be preferentially adsorbed in the pores of MFU-4l at the expense of acetone. On the contrary, MIL-100(Al) exhibits some coordinated water molecules grafted on Al(III) octahedra from the framework. One could suspect therefore acetone to be more easily bound to the Aluminium Lewis acid sites, through its C=O bond, than methanol.[39] These hypotheses will however need to be validated by additional experiments beyond the scope of this study.

Conclusions

In conclusion, this article demonstrates for the first time that Fe(II) coordination complexes can be anchored on robust MOF SBUs using a sequential installation strategy. The coordination sphere around Fe(II) could be modulated upon sorption of alcohols in the pores of the MOF, leading to a reversible colour change from orange to red, while the anchoring of the complex with coordination bonds ensured that no leaching occurred in the dispersion. In the case of MFU-4l, a preferential adsorption of MeOH compared to acetone has been observed, evidencing the fact that the host matrix can be beneficial for pre-concentrating a targeted analyte. The application of this strategy to additional SCO complexes/MOFs compositions is underway, aiming at getting a more systematic understanding on how the properties of the guest complexes can be modulated by solvent sorption. In the following step, the switching properties of these solids in presence of VOCs vapors will be investigated. Considering the increasing number of highly porous water stable diamagnetic MOFs bearing open metal sites, and the diversity of SCO complexes, this creates opportunities for the design of a new generation of VOCs sensing devices.

Experimental

PXRD: Powder X-ray Diffraction data were recorded on a high-throughput Bruker D8 Advance diffractometer working on transmission mode and equipped with a focusing Göbel mirror producing CuKα radiation (λ = 1.5418 Å) and a LynxEye detector.

SC-XRD: Single crystal X-ray Diffraction data were recorded on a four-circle kappa-axis Bruker D8 Venture diffractometer equipped with a Mo microsource and photon III detector.

N_2 adsorption: N_2 sorption measurements were performed at 77 K on Micromeretics Tristar or Triflex apparatus. The samples (ca. 40 mg) were activated by heating the powder at 120 °C (MIL-100(Al)) or 170°C (MFU-4l) under secondary vacuum for 12 h.

SEM-EDS: SEM images were recorded with FEI Magellan 400 scanning electron microscope equipped with and Oxford EDS probe.

UV-Vis: The optical spectra on solids and suspensions have been measured with a Varian Cary 300 Bio UV-Vis spectrometer equipped with an integration sphere in diffuse reflectance mode. In the case of the suspensions, concentration of ca. 1mg of solid/mL has been used. VT measurements in solution were performed with a Varian Cary 60 spectrophotometer equipped with a Hellma immersion probe (1 cm optical pathlength) and a fiber-optic cable. Low temperature was maintained using a Thermo Haake CT90L cryostat.

TGA: TGA were performed on Mettler Toledo TGA/DSC 1, STAR®System apparatus under N_2 atmosphere, at a heating rate of 5 °C.min^{-1} up to 600 °C.

Materials

All reactants were purchased from commercial suppliers and used without further purification.

Preparation of MFU-4l. MFU-4l was prepared by scaling up a previously reported procedure.[40] BTDD (1g, 3.76 mmol) was dissolved in refluxing DMF. The obtained solution was cooled down to room temperature and anhydrous zinc chloride (10.28 g, 75.43 mmol) was added. The resulting suspension was stirred under reflux for 16 hours. The precipitate was isolated by filtration while hot and washed sequentially with hot DMF (2*100 mL) then MeOH (3*50 mL) and DCM (50 mL) and dried under vacuum. Formula: Zn5(BTDD)3Cl4

Preparation of MIL-100(Al). $Al(NO_3)_3.9H_2O$ (1.5 g, 4.0 mmol) and trimesic acid (1.26 g, 6.0 mmol) and distilled water (25 mL) were added in a 100 mL capacity microwave reactor (Mars) and the resulting suspension was stirred at room temperature for 5 minutes. The reactor was sealed and the reaction mixture was heated to 210°C (1200 W) within a 1 minute ramp then kept at this temperature for 5 minutes under strong stirring. Immediately after reaction, the reactor was promptly cooled down using a water/ice bath. The white microcrystalline precipitate was isolated by filtration, washed with 100 mL of H_2O, then 100 mL of EtOH and dried in air. Finally the solid was resuspended in 125 mL EtOH and heated under reflux for 3 hours, then filtered and dried in air. Formula: $Al_3O(OH)(H_2O)_2(BTC)_2.12H_2O$

BPI.Li. 2,6-bis(1H-pyrazol-1-yl)isonicotinic acid (HBPI) was prepared according to a previously reported procedure.[41] BPI.Li, the lithium salt of HBPI, was prepared by refluxing a solution of HBPI

(2.0 g, 7.83 mmol) and LiOH (188 mg, 7.83 mmol) in MeOH (500 mL) for 1 h, followed by evaporation of the solvent under reduced pressure, recrystallization from EtOH/petroleum ether 60-40, filtration and drying in air.

BPI⊂MFU-4l. Dried MFU-4l (0.5 g, 0.4 mmol) was suspended in 100 mL of MeOH and a solution of BPI.Li (210 mg, 0.8 mmol) in MeOH (100 mL) was slowly added over 1 day. The resulting mixture was stirred at room temperature for 16 h. The solid was isolated by filtration, washed with MeOH (3*50 mL) and dried in air. BPI loading was determined by liquid ^{1}H NMR of the acid digested functionalized MOF (see SI) and confirmed by EDS and TGA. Formula: $Zn_5(BTDD)_3(BPI)_2Cl_2$

BPI⊂MIL-100(Al). Hydrated MIL-100(Al) (0.2 g, 0.26 mmol) and BPI.Li (0.2 g, 0.77 mmol) were added to EtOH (100 mL) and the resulting mixture was refluxed for 16 h. The solid was isolated by filtration, washed with EtOH (3*50 mL) and dried in air. BPI loading was determined by liquid ^{1}H NMR of the acid digested functionalized MOF (see SI) and confirmed by EDS and TGA. Formula: $Al_3O(OH)_{0.4}(H2O)_2(BTC)_2(BPI)_{0.6}$

1⊂MFU-4l. MFU-4l_BPI (50 mg, 0.03 mmol) and $Fe(ClO_4)_2.xH_2O$ (23 mg) were added to EtOH (10 mL) and the suspension was stirred for 30 min, then a solution of BPI (12 mg, 0.05 mmol) in EtOH (10 mL) was added and the suspension was stirred for 16 h. The solid was isolated by centrifugation, then washed with acetone (2*20 mL) and dried in air. BPI and Fe loadings were determined by liquid ^{1}H NMR of the acid digested functionalized MOF (see SI) and confirmed by EDS and TGA. Formula: $Zn_5(BTDD)_3Cl_2[(BPI)_2Fe_2(HBPI)_{1.5}(ClO_4)_4]$

1⊂MIL-100(Al). MIL-100(Al)_BPI (50 mg, 0.08 mmol) and $Fe(ClO_4)_2.xH_2O$ (20 mg) were added to EtOH (10 mL) and the suspension was stirred for 30 min, then a solution of BPI (12 mg, 0.05 mmol) in EtOH (10 mL) was added and the suspension was stirred for 16 h. The solid was isolated by centrifugation, then washed with acetone (2*20 mL) and dried in air. BPI and Fe loadings were determined by liquid ^{1}H NMR of the digested functionalized MOF (see SI) and confirmed by EDS and TGA. Formula: $Al_{2.67}Fe_{0.33}O(OH)_{0.4}(H_2O)_2(BTC)_2[(BPI)_{0.6}Fe_{0.6}(HBPI)_{0.51}(ClO_4)_{1.2}]$

Conflicts of interest

There are no conflicts to declare.

Acknowledgements

The authors thank the ANR MOFSCO (ANR-18-CE09-0005-01) for funding. P. Chandra, G. Mouchaham, F. Nouar and J. Sun are thanked for their help on MOF synthesis

Notes and references

(1) Zhou, X.; Lee, S.; Xu, Z.; Yoon, J. Chem. Rev. 2015, 115 (15), 7944–8000.

(2) Wales, D. J.; Grand, J.; Ting, V. P.; Burke, R. D.; Edler, K. J.; Bowen, C. R.; Mintova, S.; Burrows, A. D. Chem. Soc. Rev. 2015, 44 (13), 4290–4321.

(3) Vellingiri, K.; Szulejko, J. E.; Kumar, P.; Kwon, E. E.; Kim, K.-H.; Deep, A.; Boukhvalov, D. W.; Brown, R. J. C. Sci Rep 2016, 6 (1), 27813.

(4) Bahri, M.; Haghighat, F.; Kazemian, H.; Rohani, S. A Chemical Engineering Journal 2017, 313, 711–723.

(5) Xie, L.-H.; Liu, X.-M.; He, T.; Li, J.-R. Chem 2018, 4 (8), 1911–1927.
(6) Wang, H.; Lustig, W. P.; Li, J. Chem. Soc. Rev. 2018, 47 (13), 4729–4756.
(7) Ohba, M.; Yoneda, K.; Agustí, G.; Muñoz, M. C.; Gaspar, A. B.; Real, J. A.; Yamasaki, M.; Ando, H.; Nakao, Y.; Sakaki, S.; Kitagawa, S. Angew. Chem. Int. Ed. 2009, 48 (26), 4767–4771.
(8) Kreno, L. E.; Leong, K.; Farha, O. K.; Allendorf, M.; Van Duyne, R. P.; Hupp, J. T. Chem. Rev. 2012, 112 (2), 1105–1125.
(9) Shao, F.; Li, J.; Tong, J.-P.; Zhang, J.; Chen, M.-G.; Zheng, Z.; Huang, R.-B.; Zheng, L.-S.; Tao, J. Chem. Commun. 2013, 49 (91), 10730.
(10) Coronado, E.; Giménez-Marqués, M.; Mínguez Espallargas, G.; Rey, F.; Vitórica-Yrezábal, I. J. J. Am. Chem. Soc. 2013, 135 (43), 15986–15989.
(11) Yi, F.-Y.; Chen, D.; Wu, M.-K.; Han, L.; Jiang, H.-L. ChemPlusChem 2016, 81 (8), 675–690.
(12) Ni, Z.-P.; Liu, J.-L.; Hoque, Md. N.; Liu, W.; Li, J.-Y.; Chen, Y.-C.; Tong, M.-L. Coordination Chemistry Reviews 2017, 335, 28–43..
(13) Mínguez Espallargas, G.; Coronado, E. Chem. Soc. Rev. 2018, 47 (2), 533–557.
(14) Burtch, N. C.; Jasuja, H.; Walton, K. S. Chem. Rev. 2014, 114 (20), 10575–10612.
(15) Bigdeli, F.; Lollar, C. T.; Morsali, A.; Zhou, H. Angew. Chem. Int. Ed. 2020, 59 (12), 4652–4669.
(16) Real, J. A.; Gaspar, A. B.; Muñoz, M. C. Thermal, Dalton Trans. 2005, No. 12, 2062.
(17) Sieber, R.; Decurtins, S.; Stoeckli-Evans, H.; Wilson, C.; Yufit, D.; Howard, J. A. K.; Capelli, S. C.; Hauser, A. Chem. Eur. J. 2000, 6 (2), 361–368.
(18) Krivokapic, I.; Zerara, M.; Daku, M. L.; Vargas, A.; Enachescu, C.; Ambrus, C.; Tregenna-Piggott, P.; Amstutz, N.; Krausz, E.; Hauser, A. Coordination Chemistry Reviews 2007, 251 (3–4), 364–378.
(19) Clemente-León, M.; Coronado, E.; López-Jordà, M.; Waerenborgh, J. C.; Desplanches, C.; Wang, H.; Létard, J.-F.; Hauser, A.; Tissot, A. J. Am. Chem. Soc. 2013, 135 (23), 8655–8667.
(20) Abhervé, A.; Grancha, T.; Ferrando-Soria, J.; Clemente-León, M.; Coronado, E.; Waerenborgh, J. C.; Lloret, F.; Pardo, E. Chem. Commun. 2016, 52 (46), 7360–7363.
(21) Zhao, T.; Boldog, I.; Spasojevic, V.; Rotaru, A.; Garcia, Y.; Janiak, C. J. Mater. Chem. C 2016, 4 (27), 6588–6601.
(22) López-Jordà, M.; Giménez-Marqués, M.; Desplanches, C.; Mínguez Espallargas, G.; Clemente-León, M.; Coronado, E. Eur. J. Inorg. Chem. 2016, 2016 (13–14), 2187–2192.
(23) Tissot, A.; Kesse, X.; Giannopoulou, S.; Stenger, I.; Binet, L.; Rivière, E.; Serre, C. Chem. Commun. 2019, 55 (2), 194–197.
(24) Cohen, S. M. Chem. Rev. 2012, 112 (2), 970–1000..
(25) Islamoglu, T.; Goswami, S.; Li, Z.; Howarth, A. J.; Farha, O. K.; Hupp, J. T. Acc. Chem. Res. 2017, 50 (4), 805–813.
(26) Abhervé, A.; Clemente-León, M.; Coronado, E.; Gómez-García, C. J.; López-Jordà, M. Dalton Trans. 2014, 43 (25), 9406–9409.
(27) García-López, V.; Palacios-Corella, M.; Abhervé, A.; Pellicer-Carreño, I.; Desplanches, C.; Clemente-León, M.; Coronado, E. Dalton Trans. 2018, 47 (47), 16958–16968.
(28) Halcrow, M. A. Coordination Chemistry Reviews 2009, 253 (21–22), 2493–2514.
(29) Barrett, S. A.; Kilner, C. A.; Halcrow, M. A. Dalton Trans. 2011, 40 (45), 12021.
(30) Kershaw Cook, L. J.; Mohammed, R.; Sherborne, G.; Roberts, T. D.; Alvarez, S.; Halcrow, M. A. Coordination Chemistry Reviews 2015, 289–290, 2–12.
(31) Halcrow, M. A.; Capel Berdiell, I.; Pask, C. M.; Kulmaczewski, R. Inorg. Chem. 2019, 58 (15), 9811–9821.

(32) Denysenko, D.; Grzywa, M.; Tonigold, M.; Streppel, B.; Krkljus, I.; Hirscher, M.; Mugnaioli, E.; Kolb, U.; Hanss, J.; Volkmer, D. Chem. Eur. J. 2011, 17 (6), 1837–1848.
(33) Volkringer, C.; Popov, D.; Loiseau, T.; Férey, G.; Burghammer, M.; Riekel, C.; Haouas, M.; Taulelle, F. Chem. Mater. 2009, 21 (24), 5695–5697.
(34) García Márquez, A.; Demessence, A.; Platero-Prats, A. E.; Heurtaux, D.; Horcajada, P.; Serre, C.; Chang, J.-S.; Férey, G.; de la Peña-O'Shea, V. A.; Boissière, C.; Grosso, D.; Sanchez, C. Eur. J. Inorg. Chem. 2012, 2012 (32), 5165–5174.
(35) Kershaw Cook, L. J.; Kulmaczewski, R.; Mohammed, R.; Dudley, S.; Barrett, S. A.; Little, M. A.; Deeth, R. J.; Halcrow, M. A. A Unified Treatment of the Relationship Between Ligand Substituents and Spin State in a Family of Iron(II) Complexes. Angew. Chem. Int. Ed. 2016, 55 (13), 4327–4331. https://doi.org/10.1002/anie.201600165.
(36) Nikovskiy, I.; Polezhaev, A.; Novikov, V.; Aleshin, D.; Pavlov, A.; Saffiulina, E.; Aysin, R.; Dorovatovskii, P.; Nodaraki, L.; Tuna, F.; Nelyubina, Y. Chem. Eur. J. 2020, chem.202000047.
(37) Jeremias, F.; Khutia, A.; Henninger, S. K.; Janiak, C. J. Mater. Chem. 2012, 22 (20), 10148–10151.
(38) Wright, A. M.; Rieth, A. J.; Yang, S.; Wang, E. N.; Dincă, M. Chem. Sci. 2018, 9 (15), 3856–3859.
(39) Horcajada, P.; Serre, C.; Vallet-Regí, M.; Sebban, M.; Taulelle, F.; Férey, G. Angew. Chem. Int. Ed. 2006, 45 (36), 5974–5978.
(40) Denysenko, D.; Grzywa, M.; Tonigold, M.; Streppel, B.; Krkljus, I.; Hirscher, M.; Mugnaioli, E.; Kolb, U.; Hanss, J.; Volkmer, D. Chem. Eur. J. 2011, 17 (6), 1837–1848.
(41) Klein, C.; Baranoff, E.; Grätzel, M.; Nazeeruddin, Md. K. Tetrahedron Letters 2011, 52 (5), 584–587.